IOP Publishing Phys. Med. Biol. 70 (2025) 075018 https://doi.org/10.1088/1361-6560/adc234

Physics in Medicine & Biology

IPEM Institute of Physics and Engineering in Medicine

OPEN ACCESS

RECEIVED
16 October 2024

REVISED
2 March 2025

ACCEPTED FOR PUBLICATION
18 March 2025

PUBLISHED
27 March 2025

PAPER

Radiation damage and recovery of plastic scintillators under ultra-high dose rate 200 MeV electrons at CERN CLEAR facility

Cloé Giguère[1,2], Alexander Hart[3], Joseph Bateman[4], Pierre Korysko[4,5], Wilfrid Farabolini[5], Yoan LeChasseur[6], Magdalena Bazalova-Carter[3,*] and Luc Beaulieu[1,2]

[1] Département de Physique, de Génie Physique et d'Optique et Centre de Recherche sur le Cancer, Université Laval, Québec, QC G1V 0A6, Canada
[2] Département de Radio-Oncologie et Axe Oncologie du CRCHU de Québec, CHU de Québec, Université Laval, Québec, QC G1V 0A6, Canada
[3] Department of Physics and Astronomy, University of Victoria, Victoria, BC V8P 5C2, Canada
[4] Department of Physics, University of Oxford, OX1 3AZ Oxford, United Kingdom
[5] CERN, 1211 Geneva, Switzerland
[6] Medscint, Québec, QC, Canada
[*] Author to whom any correspondence should be addressed.

E-mail: bazalova@uvic.ca

Keywords: FLASH, ultra-high dose rate (UHDR) radiotherapy, very high energy electrons (VHEE), radiation damage, plastic scintillation dosimeter (PSD), scintillation dosimetry, optical fiber dosimetry

Abstract

Objective. The FLASH effect holds significant potential in improving radiotherapy treatment outcomes. Very high energy electrons (VHEEs) with energies in the range of 50–250 MeV can effectively target tumors deep in the body and can be accelerated to achieve ultra-high dose rates (UHDR), making them a promising modality for delivering FLASH radiotherapy in the clinic. However, apart from suitable VHEE sources, clinical translation requires accurate dosimetry, which is challenging due to the limitation of standard dosimeters under UHDR conditions. In this study, water-equivalent and real-time plastic scintillation dosimeters (PSDs) are tested to evaluate their viability for FLASH VHEE dosimetry. *Approach.* A 4-channel PSD, consisting of polystyrene-based BCF12 and Medscint proprietary scintillators, polyvinyltoluene-based EJ-212 and a blank plastic fiber channel for Cherenkov subtraction was exposed to the 200 MeV VHEE UHDR beam at the CLEAR CERN facility. The Hyperscint RP200 platform was used to assess linearity to dose pulses of up to 90 Gy and dose rates up to 4.6×10^9 Gy s^{-1}, and to investigate radiation damage and recovery after dose accumulation of 37.2 kGy. *Main results.* While blank fiber response was linear across the entire dose range studied, light output saturated above 45 Gy/pulse for scintillators. Despite radiation damage, linearity was preserved, though it resulted in a decrease of scintillator and blank fiber light output of $<$1.87%/kGy and a shift in spectra towards longer wavelengths. Short-term recovery ($<$100 h) of these changes was observed and depended on rest duration and accumulated dose. After long-term rest ($<$172 days), light output recovery was partial, with 6%–22% of residual permanent damage remaining, while spectral recovery was complete. *Significance.* We showed that PSDs are sensitive to radiation damage, but maintain dose linearity even after a total accumulated dose of 37.2 kGy, and exhibit significant response recovery. This work highlights the potential of PSDs for dosimetry in UHDR conditions.

1. Introduction

Despite modern advancements in radiation therapy, curative doses delivered to the tumour are still limited by normal tissue tolerance to radiation, motivating research into new radiotherapy techniques. One promising approach is the use of ultrahigh dose rate (UHDR) radiation beams to trigger the FLASH effect; a reduction in radiation toxicity to healthy tissue while preserving tumor control (Favaudon *et al* 2014). The FLASH

effect has been observed in multiple animal models (Montay-Gruel *et al* 2017, 2019, Vozenin *et al* 2019) and its clinical feasibility has been demonstrated in human patients (Bourhis *et al* 2019, Mascia *et al* 2023).

Most of the FLASH preclinical studies utilize electrons in the energy range of 4–25 MeV. While photons are the standard of care in the clinic, producing them at UHDR is technically difficult due to the low electron to photon bremsstrahlung conversion efficiency (Esplen *et al* 2022, Yang *et al* 2024). Protons, with their favorable Bragg peak shaped dose distribution and their ability to penetrate deep in the patient, are a promising modality for FLASH RT, but also face significant technical hurdles for delivery at UHDR, as well as being sensitive to tissue heterogeneities and patient motion (Jolly *et al* 2020, Sarti *et al* 2021, Whitmore *et al* 2021, Diffenderfer *et al* 2022). In spite of their wide use, electrons in the 4–25 MeV range have important drawbacks; they have low penetration in tissue, thus making them ill-suited for the treatment of deep-seated tumours, and have large lateral penumbras (DesRosiers *et al* 2000, Zhang *et al* 2023).

Very high energy electrons (VHEEs) of energies in the range 100–250 MeV are an attractive alternative to the previous modalities, with their broad peak dose distribution that can reach deep in the body (>20 cm) and their lower sensitivity to inhomogeneities compared to proton or photon beams (Whitmore *et al* 2021, Clements *et al* 2023, Fischer *et al* 2024). VHEEs scatter less in air than low energy electrons, have sharp penumbras comparable to photon beams (DesRosiers *et al* 2000, Grazia Ronga *et al* 2021, Tobias Böhlen *et al* 2021), and they can be scanned to produce similar or better dose distributions than clinical Volumetric Modulated Arc Therapy plans (Bazalova-Carter *et al* 2015). Alternatively, VHEEs can be focused to achieve similar target coverage compared to spread-out Bragg peak proton beams (Whitmore *et al* 2021). While current accelerator technology does not allow the delivery of VHEEs in a clinical setting, compact machines with high accelerating gradients ($\approx$100 MeV m^{-1}) using X-band radiofrequency electron acceleration cavities have been proposed by the CHUV-CERN collaboration and SLAC National Accelerator Laboratory (Vozenin *et al* 2022, Schulte *et al* 2023, Bateman *et al* 2024). In addition to their favorable properties, VHEEs can be delivered at high fluxes, making them promising candidates for translating FLASH radiotherapy into clinical practice.

VHEE UHDRs bring new dosimetric challenges due to the high doses delivered in each very short pulse. An ideal dosimeter for UHDR applications should possess the following characteristics (Ashraf *et al* 2020, Romano *et al* 2022): dose rate independence ranging from conventional to UHDR regimes (>10^5 Gy s^{-1}), high temporal resolution for real-time dose monitoring, high spatial resolution for small field measurements characteristic of many FLASH-capable machines and a wide dynamic range to measure the high single doses used in FLASH treatments (about 8–15 Gy at the moment for human patients in studies by Bourhis *et al* 2019 and Mascia *et al* 2023). Most preclinical studies have used radiochromic films (Bourhis *et al* 2019, Vozenin *et al* 2019, Ashraf *et al* 2022), that allow 2D dose measurements with high spatial resolution, and alanine (Bourhis *et al* 2019, Vozenin *et al* 2019) for dosimetry in FLASH conditions (Esplen *et al* 2020). Thermo-luminescent dosimeters have also been used in a few studies (Jorge *et al* 2019, Vozenin *et al* 2019). While these dosimeters demonstrate excellent dose-rate independence (Karsch *et al* 2012, Jaccard *et al* 2017, Jorge 2019, Romano *et al* 2022), they can only give an offline measure of dose after irradiation (Andreo *et al* 2017). In conventional clinical settings, where mean dose rates are around 0.1 Gy s^{-1}, ionization chambers are the reference dosimeter for real-time dosimetry. However, significant saturation of their response due to a decrease in ion collection efficiency limit their usability in UHDR conditions (Petersson *et al* 2017, Ashraf *et al* 2020, Bourgouin *et al* 2020, McManus *et al* 2020, Poppinga *et al* 2020), although these effects have been shown to be reduced using new ion chamber designs with smaller electrode separation and higher bias voltage (Liu *et al* 2024).

Small sized and fast plastic scintillation dosimeters (PSDs), with their excellent water equivalence and energy independence (Beaulieu and Beddar 2016, Beddar and Beaulieu 2016), could offer a viable solution for accurate dosimetry for UHDR treatments. While dosimetric performances of PSDs are well characterized in conventional dose rates for different applications including small field dosimetry and brachytherapy (Beaulieu *et al* 2013, Beaulieu and Beddar 2016, Beddar and Beaulieu 2016), many uncertainties persist regarding their performance in UHDR conditions. Application of PSDs to UHDR beams has been investigated in a few studies with synchrotron x-rays at about 4000 Gy s^{-1} (Archer *et al* 2019), 120 kVp x-rays up to 40 Gy s^{-1} (Cecchi *et al* 2021, Hart *et al* 2022), 16 MeV electrons at 100 Gy s^{-1} (Poirier *et al* 2022), 10 MeV electrons up to 350 Gy s^{-1} (Ashraf *et al* 2022), 9 MeV electrons with instantaneous dose rates (IDR) over 10^6 Gy s^{-1} (Ciarrocchi *et al* 2024), 9 MeV electrons up to 876 Gy s^{-1} (Liu *et al* 2024) and 200 MeV VHEEs with IDRs up to 10^9 Gy s^{-1} (Hart *et al* 2024). These studies suggest that PSDs exhibit linear response to dose per pulse and are dose rate independent for FLASH dose rates. However, saturation of scintillator response at high doses per pulse was observed by Hart *et al* (2024) with VHEEs, leading to a loss of linearity above 125.2 and 59.5 Gy/pulse respectively for BCF12 and Medscint scintillators. Additional research on this phenomenon needs to be conducted. Moreover, one important drawback on the use of PSDs for UHDR dosimetry is the decrease of scintillator response ranging from $\sim$1.2 to 16.2%/kGy that occurs

with radiation damage after accumulation of high doses, which was reported by three recent studies (Ashraf *et al* 2022, Hart *et al* 2024, Liu *et al* 2024).

Building on previous works by Hart *et al* (2024) and Giguère *et al* (2024), this paper expands on the application of PSDs to UHDR VHEEs by further investigating the linearity and radiation damage of PSDs. Additionally, it examines the short and long-term recovery of the spectral and output responses of three different plastic scintillators as well as a blank plastic optical fiber.

2. Methods

2.1. CLEAR beamline

Measurements using VHEEs presented in this work were acquired at the CERN Linear Electron Accelerator for Research (CLEAR) facility that houses a 60–220 MeV electron beam (Sjobak *et al* 2019). The beam has a time structure composed of bunches and bunch trains, referred to as 'pulses' throughout this article. Bunches are groups of electrons of 0.1–10 ps in length and 2-nC maximal charge, sent out at a frequency of 1.5 or 3 GHz. Groups of up to 400 bunches form pulses with a total charge of up to 80 nC. Pulse repetition frequency can be adjusted between 0.833 to 10 Hz to vary the mean or average dose rate, defined as the product of the dose per pulse and the number of pulses divided by the total irradiation time. IDRs or the dose rates within a single pulse, were calculated by dividing the pulse dose by the pulse duration, which was determined by the bunch frequency and the number of bunches per pulse. The beamline produces a small Gaussian beam, of about 15 mm at full width half maximum (FWHM) in water, using a yttrium aluminium garnet (YAG) scatterer and quadrupoles magnets upstream of the vacuum window. An integrating current transformer (ICT) measures the delivered charge per pulse after the vacuum window. While an energy of 200 MeV was targeted, beam energy of (200 ± 5 MeV) was delivered for all the measurements at the CLEAR beamline.

2.2. Experimental setups

A 4-channel PSD apparatus presented in figure 1(a) was designed with polystyrene based BCF-12 scintillating fiber (Luxium Solutions, Hiram, USA), polyvinyltoluene (PVT) based EJ-212 scintillator (Eljen Technology, Sweetwater, USA), polystyrene based proprietary Medscint scintillator (Medscint Inc. Quebec, Canada) and poly (methyl methacrylate) (PMMA) optical fiber (Super Eska SH2002, Mitsubishi Chemical Group, Tokyo, Japan). All scintillators have an emission spectra mainly in the blue region of the electromagnetic spectrum, with peak emission at 435, 423 and 425 nm respectively for BCF-12, EJ-212 and Medscint. Scintillators were coupled independently to PMMA optical fibers (Super Eska SH2002, Mitsubishi Chemical Group, Tokyo, Japan) using optical grade epoxy glue after polishing each surface. The fourth channel, a blank fiber without a scintillating element, was used to subtract stem effect light, composed of Cherenkov and fluorescence, from the scintillator signals. The 4-channel PSD was encased in a black opaque sheath to eliminate ambient light contamination. For VHEEs measurements at CLEAR, the probe was installed on a 3D printed holder held by the C-Robot (Korysko n.d.) in a water tank, as shown in figure 1(b). Positioning of the PSD apparatus at the center of the Gaussian beam was done visually, using a YAG scintillating screen behind the probe. When irradiated, the YAG screen produced scintillating light that was reflected by a 45° mirror towards a camera. This allowed the measurement of the beam size at the longitudinal position of the PSD in water. The presence of the PSD in front of the YAG screen produced a shadow on the light captured by the camera, allowing for the visualization of the transverse position of the probe with respect to the beam. Positioning adjustments were made using the C-Robot to visually align the 4-channel PSD at the center of the beam.

To study long-term recovery, reference experiments were also performed with a TrueBeam Linac (Varian Medical Systems, Palo Alto, USA) before and after CLEAR experiments. PSD data were acquired using the TrueBeam 6 MV photon treatment beam and the 90 kVp on-board imager x-ray tube. For 6 MV measurements, the probe was placed between two 10 cm solid water slabs at the machine isocenter, and irradiated with a 10×10 cm^2 field of 500 MUs. For the 90 kV measurements, the probe was taped directly at the center of the exit window of the kV tube, operated at tube current of 154 mA and exposure time of 180 ms. Cumulative dose delivered to the PSD during each measurement session was kept below 50 Gy to limit the increase of the total accumulated dose.

For all experiments, the 4 channels were connected independently to the Medscint Hyperscint RP200 (Medscint Inc. Quebec, Canada) dosimetry platform to measure spectral response at a frequency of 8.33 Hz.

2.3. Radiochromic film dosimetry

For measurements at the CLEAR beamline, targeted doses per pulse were calculated using the pulse charge, measured by the ICT, and the beam size. Actual delivered doses per pulse were obtained using Gafchromic MD-V3 films (Ashland Inc. Wilmington, USA). Calibration films were irradiated using the 5.5 MeV electron beam of an eRT6 Oriatron (PMB-Alcen, Peynier, France) with duplicate exposures to doses ranging from 0

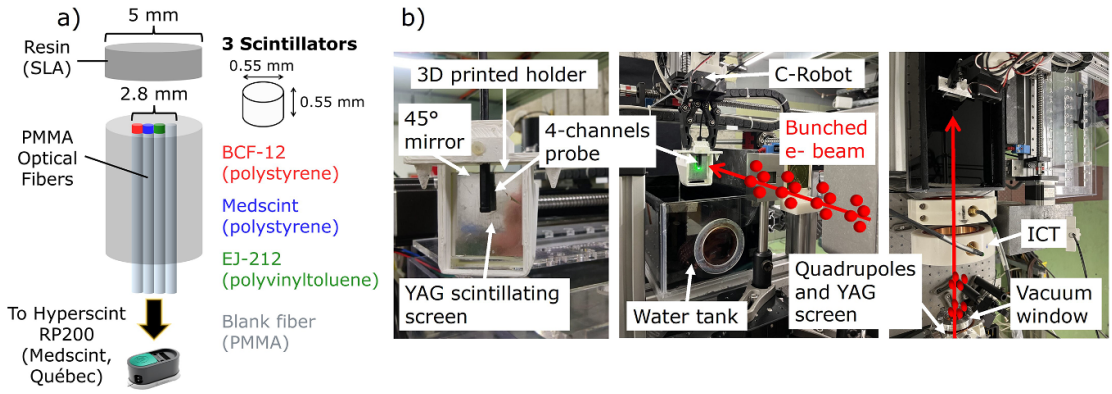

Figure 1. (a) Schematic of the 4-channel PSD and (b) experimental setup on the in-air test stand of the CLEAR beamline.

to 200 Gy. Red channel mean pixel value of the center region of interest (ROI) in each film was plotted according to dose delivered and then fitted with a rational function, as described in Santos *et al* (2021). This calibration curve was then used to convert pixel value to dose for film measurements during the experiments.

Two to four film measurements were performed on each experimental day to allow for daily charge to dose conversion. In addition, a background film was kept in the irradiation hall for each measurement set. Films were scanned approximately 24 h after irradiation, using a Perfection V800 Photo scanner (Epson, Suwa, Japan) with a resolution of 300 dpi. Background subtracted films were converted to dose using the red channel pixel value to dose calibration curve. Mean values of a 1×1 mm^2 ROI in the beam center of each films were plotted according to ICT measured charges and linear regressions were performed for each day of measurements. The use of a different charge to dose calibration on each experimental day allowed to account for changes in beam delivery throughout the days of experiment, ranging from May 17 to May 26, 2023.

2.4. CLEAR PSD measurements

Linearity of PSD output to dose per pulse was verified, with doses ranging from ∼5 to 90 Gy. Three single pulses were delivered per dose value to allow calculation of the mean and standard deviation. Dose rates in pulse varied non linearly with charge throughout and ranged from 2.2×10^8 to 4.6×10^9 Gy s^{-1}. Linearity of response to dose was assessed by plotting area under the curve (AUC) of background-subtracted spectra according to dose per pulse. Linear regressions were computed on the data, excluding data points where response saturated, i.e. data points above the saturation limit. To determine the saturation limit for each linearity measurement, linear regressions were first performed using only the data points corresponding to the three lowest dose values. The saturation limit was identified as the highest dose per pulse included in the regression at which the fit remained representative of the data below that threshold. This was primarily assessed using the calculated 95% confidence bands around the regressions. Data points falling outside these confidence bands were considered saturated and excluded from the final regressions. Saturation limits were confirmed based on the goodness of fit; regressions with $R^2<0.97$ were considered invalid and saturation limits were lowered until the $R^2>0.97$.

Slopes of linear regressions were taken as light output and tracked based on accumulated dose to assess radiation damage. In between linearity measurements, the 4-channel PSD was damaged with irradiations of ∼5 kGy delivered with about 12 Gy pulses at 3.33 Hz for mean dose rate of ∼40 Gy s^{-1} and IDR of $\sim1.4\times10^9$ Gy s^{-1}. In total, 37.2 kGy was delivered to the probe throughout the two weeks of measurements. Short-term recovery of light output and spectral response was evaluated by resting the probe for a specified amount of time ranging from 1 to 96 h after a linearity measurement, then repeating the measurement to observe any changes in the response. To quantify spectral changes, the spectral centroid, or center of mass of the spectrum, was determined by calculating the weighted average of the wavelengths present in the spectrum, with the intensity values as weights.

2.5. Signal correction and uncertainty calculations

Stem-effect signal from the blank PMMA optical fiber, composed mainly of Cherenkov light, was subtracted from the scintillator signals. However, due to the Gaussian beam, not all channels received the same dose. To account for this dose variation, off-axis factors were calculated using the 2D dose distributions measured with the films, as presented in figure 2(a). The probe was assumed to be perfectly centered on the beam. While this was unlikely to be the case during the experiments, positioning uncertainty was considered later

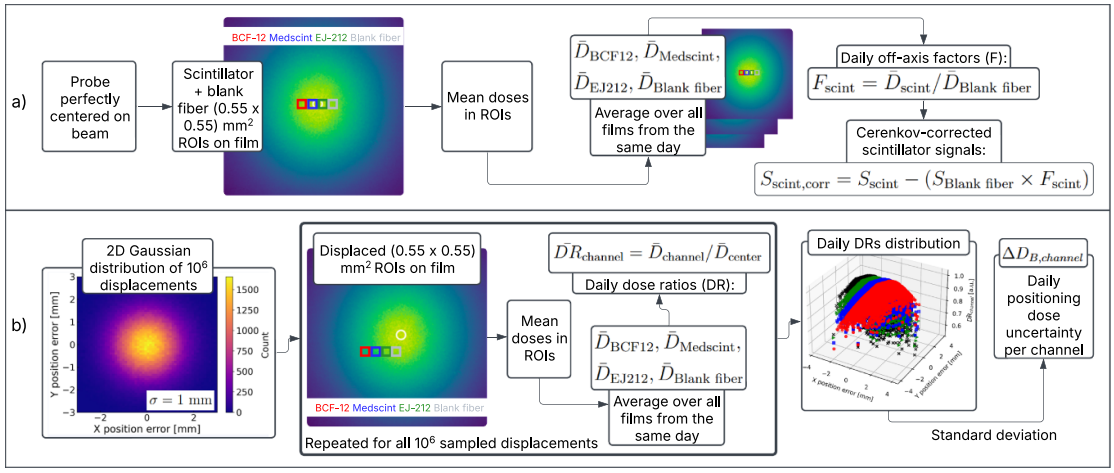

Figure 2. (a) Calculation of the daily off-axis factors (F) for correction of the Cerenkov removal. (b) Calculation of the daily positioning uncertainties ($\Delta D_{B,\text{channel}}$).

on, as described in the paragraph below. Using ROIs centered on each channel, mean film doses received by each scintillator and blank fiber were calculated and then averaged over all ROI doses from the same day. The resulting scintillator doses were divided by the blank fiber dose to determine daily off-axis factors (F), which were then multiplied to the blank fiber signal before subtraction.

To account for uncertainty in the positioning of the PSD at the center of the beam, a simulation was conducted in Python using an off-axis ratio model similar to the one described in Duchaine *et al* (2022). The calculations are schematized in figure 2(b). First, positioning errors in both directions transverse to the beam were simulated by sampling 10^6 displacements from a 2D Gaussian distribution centered at 0 with a standard deviation of 1 mm. Although positioning uncertainty was not measured experimentally, it was estimated during the measurements that most errors remained below 1 mm. This standard deviation was therefore chosen to ensure that the majority of simulated displacements stayed within this range while still allowing for some larger displacements, resulting in a generally conservative positioning uncertainty estimate. Any displacement of the PSD from the Gaussian beam center resulted in variations in the received dose and, consequently, in its output response. Thus, for each sampled positioning error, mean delivered dose to each displaced probe channel was calculated using ROIs on the film measurements. These doses were averaged across all film measurements from the same day and then normalized to the dose at the beam center, corresponding to the dose received by a perfectly aligned probe. This produced channel-specific daily 2D dose ratio distributions, illustrating how the dose received by each channel varied with displacement from the beam center. Finally, the standard deviation was calculated and taken as the normalized dose uncertainty associated with the positioning of the 4-channel PSD in the beam ($\Delta D_{B,\text{channel}}$).

The combined standard uncertainty on dose was calculated from three distinct sources: (1) Type A uncertainty calculated as the standard deviation of the three charge pulses delivered per measurement, accounting for pulse-to-pulse variations; (2) Type A uncertainties on the slope and Y-intercept of the daily charge to dose calibrations derived from film measurements; and (3) Type B positioning uncertainty previously described, following multiplication by the given dose ($\Delta D_{B,\text{channel}}$). The combined Type A uncertainty (ΔD_A) was first calculated from (1) and (2) using standard uncertainty propagation on the linear charge to dose calibration (equation (1)).

$$D = C \cdot m + b \ ; \ \Delta D_A = \sqrt{\left[(C \cdot m)\sqrt{\left(\frac{\Delta C}{C}\right)^2 + \left(\frac{\Delta m}{m}\right)^2}\right]^2 + \Delta b^2}, \tag{1}$$

where D is the pulse dose, C the pulse charge, m the slope of the daily charge to dose calibration and b its Y-intercept. The uncertainty of each parameter is denoted by Δ.

The combined standard uncertainty on dose ΔD was then calculated using the law of propagation of uncertainty combining variances, presented in equation (2) (Andreo *et al* 2017):

$$\Delta D = \sqrt{\Delta D_A^2 + \Delta D_B^2}. \tag{2}$$

2.6. Linac PSD measurements

After the measurements at the CLEAR beamline, long-term recovery was assessed by measuring output and spectra of scintillators and blank fiber at different time points (24–237 days) after radiation damage using the 6 MV and 90 kV beams of a clinical linac, as described in section 2.2. The AUC of background-subtracted spectra measured at 6 MV was used to quantify light output. To assess spectral changes, the spectral centroid of the spectra measured at 90 kV, without Cerenkov production, were calculated. All measurements were normalized to the initial light output and spectral centroid recorded under the same conditions before radiation damage. Output and spectral response were considered stabilized once a measured point fell within the error bars of the subsequent data points. To evaluate repeatability, the same measurement was repeated 10 times, each time disconnecting the probe from the Hyperscint dosimetry platform and repositioning the experimental setup. The standard deviation of the AUC across these 10 repetitions was taken as the light output uncertainty.

3. Results

3.1. Film measurements

An example of a film measurement and its associated Gaussian profiles are presented in figure 3(a) and (b), respectively. In 3(c), the variation of beam size as a function of the delivered charge for each measurement day is shown. Beam size ranged from 11.0 to 15.8 mm FWHM throughout experiments.

Charge to dose conversion factors calculated from linear regressions on the data extracted from the film measurements are reported in table 1, as well as mean FWHM over all film measurements for each day. Coefficient of determination (R^2) superior to 0.99 were computed for all linear regressions. As expected, slopes decreased with increasing beam size.

3.2. Output linearity and radiation damage

Stem effect light, composed of Cherenkov light and fluorescence, was produced in the PMMA optical fibers coupled to the scintillators. To account for the gaussian beam shape during stem effect removal, daily off-axis factors were calculated, yielding average values across all days of 1.01 (BCF-12), 1.03 (Medscint) and 1.03 (EJ-212) ($\pm$0.01). Mean contributions of stem effect light to total signal of 16, 18 and 19% ($\pm$4%) were measured throughout all measurements for BCF-12, Medscint and EJ-212 channels respectively. Stem effect contribution varied across measurement days and increased with dose per pulse.

Figure 4 compares the output linearity of all channels at the start of the experiments, after the first 1.4 kGy of accumulated dose, to the one at the end of experiments with the final accumulated dose of 37.2 kGy. For all linearity measurements, blank fiber light signal was linear over the entire range of doses per pulse and IDRs; up to 90 Gy/pulse and 4.6×10^9 Gy s^{-1}, respectively. However, the integrated scintillation signal exhibited a loss of linearity for pulses exceeding a saturation limit, averaging at (45 ± 1) Gy/pulse for all linearity measurements and the three scintillators. This dose per pulse corresponded to an IDR of approximately 8×10^8 Gy s^{-1}. An example of this saturation is noticeable in figure 4(b), where scintillator signals start deviating from the linear regressions around 45 Gy/pulse. For all the linear regressions, R^2 coefficients superior or equal to 0.97 were computed.

Figure 4 shows a significant decrease of light signal with accumulation of dose in the scintillators and blank fiber, due to radiation damage between 1.4 and 37.2 kGy. Effects of radiation damage on the light output and on the spectra, as well as short-term recovery are presented in figure 5. On average for the total dose of 37.2 kGy, loss of light yield of 1.79, 1.87, 1.67 and 1.54%/kGy ($\pm$0.03%/kGy) were measured for BCF-12, Medscint, EJ-212 and blank fiber respectively. With dose, spectra were shifted towards longer yellower wavelengths. In order of increasing accumulated dose, short-term output recovery was observed for the scintillators after 1, 96 and 26 h of rest between measurements, while spectral recovery occurred only after the 96 and 20 h rest periods. No recovery, either spectral or output, was observed following the first rest period, of 21.5 h, at an accumulated dose of 1.4 kGy.

3.3. Long-term recovery

Long-term recovery of light yield output and spectral changes at time points ranging from 24 to 237 days after radiation damage is reported in figure 6, compared to response before CLEAR irradiations.

Long-term recovery of light output loss was significant and stabilized after 32 days for BCF-12, after 150 days for Medscint, after 172 days for EJ-212 and after 32 days for blank fiber. Spectral changes fully recovered within the same timeframes for the scintillators and blank fiber, except for the EJ-212 scintillator, which showed faster spectral recovery, stabilizing after 150 days. Actual stabilization of response could have occurred anywhere within the time gap between the reported values and the previous data points.

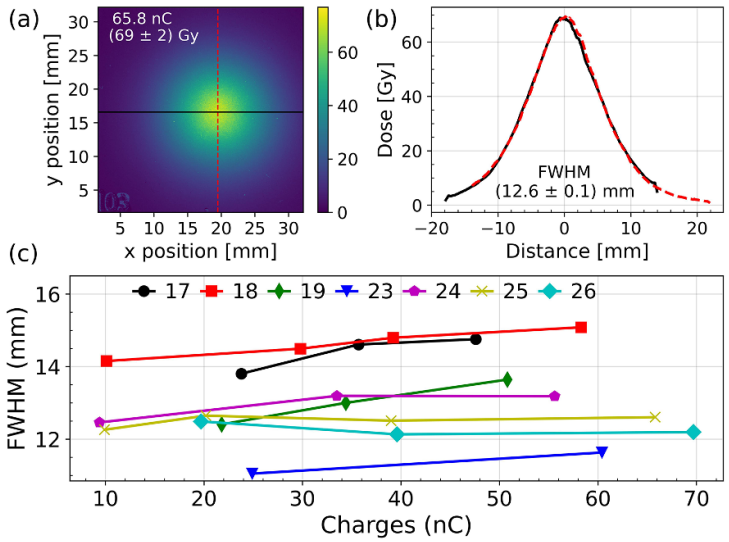

Figure 3. (a) Film measurement of a 200 MeV beam delivered at 65.8 nC and (b) beam profiles. (c) Average FWHM of beam over the x and y axis measured with MD-V3 films, for each measurement day (from May 17 to May 26).

Table 1. Dose calibration factors and beam FWHM obtained from MD-V3 film measurements.

Day (May)	Slope (Gy/nC)	Y-intercept (Gy)	FWHM (mm)
17	0.6 ± 0.1	8 ± 2	14.4 ± 0.4
18	0.74 ± 0.05	4.5 ± 0.9	14.6 ± 0.4
19	0.60 ± 0.09	12 ± 2	13.0 ± 0.5
23	1.13 ± 0.08	8 ± 3	11.3 ± 0.3
24	0.97 ± 0.04	3 ± 1	12.9 ± 0.4
25	1.01 ± 0.04	3 ± 1	12.5 ± 0.2
26	1.08 ± 0.06	5 ± 2	12.3 ± 0.2

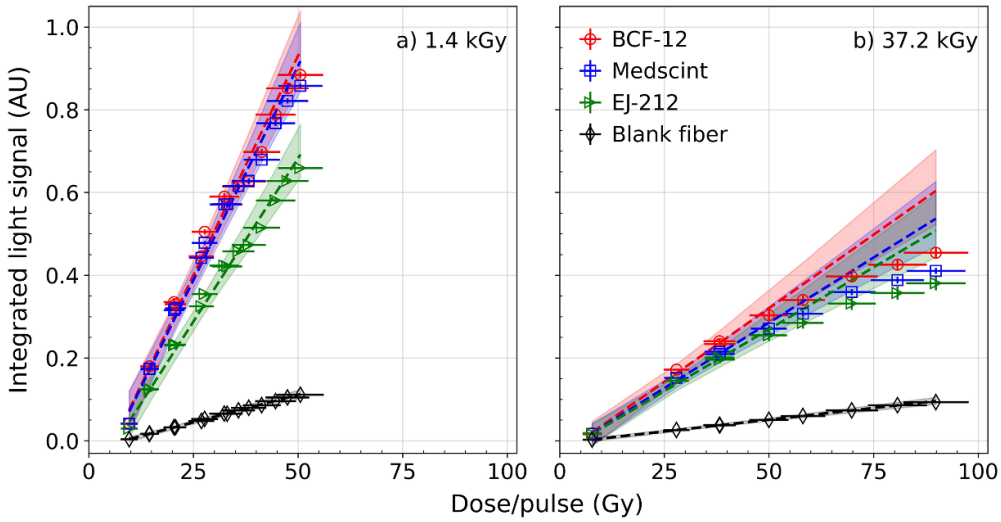

Figure 4. Linearity of AUC of scintillation and blank fiber spectra with dose per pulse, at (a) 1.4 kGy and (b) 37.2 kGy total accumulated dose in the 4-channel probe. Mean value for 3 pulses is displayed. Uncertainty in linear regressions (dashed lines) is shown with the colored shaded regions representing the 95% confidence bands.

Table 2 presents effect of radiation damage on light yield and spectral centroid during the last irradiation at CLEAR compared to the stabilized recovered response. Residual permanent damage of light output of 6–22% remains after recovery, with the Medscint scintillator being the most damaged.

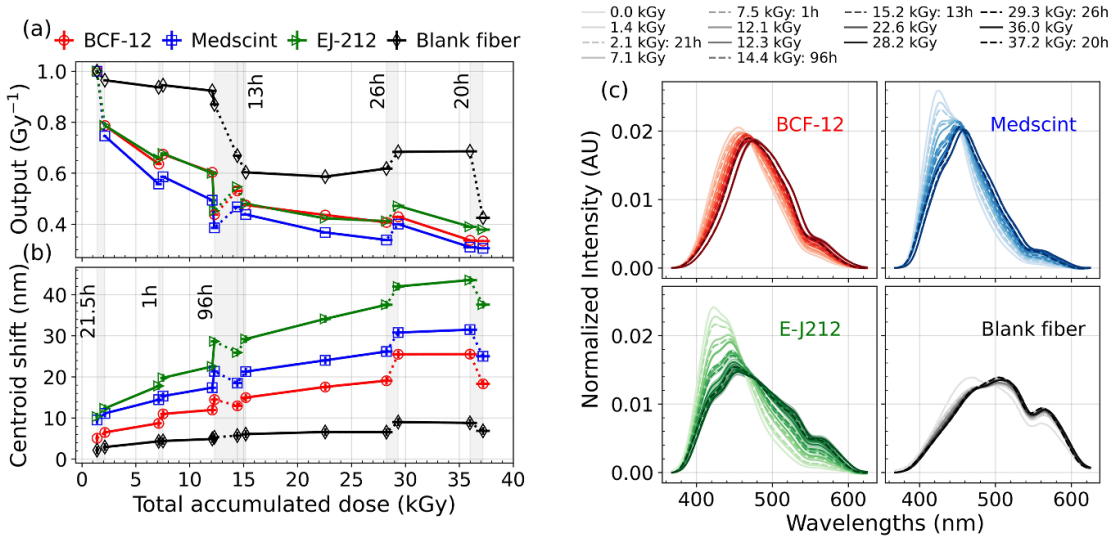

Figure 5. (a) Loss of light output of scintillators and blank fiber and (b) spectral centroid shift (compared to initial spectra) of mean scintillation spectra measured at ∼40 Gy pulses, with accumulation of dose in the 4-channel probe. Change in output and spectral centroid shift after different rest periods (from 1 h to 96 h) are displayed with dashed lines and grey shaded regions. (c) Mean spectra measured for 3 pulses of ∼40 Gy at increasing dose accumulated in the 4-channel probe, normalized by AUC. Spectra measured after different rest periods (1 h to 96 h) are displayed in dashed lines.

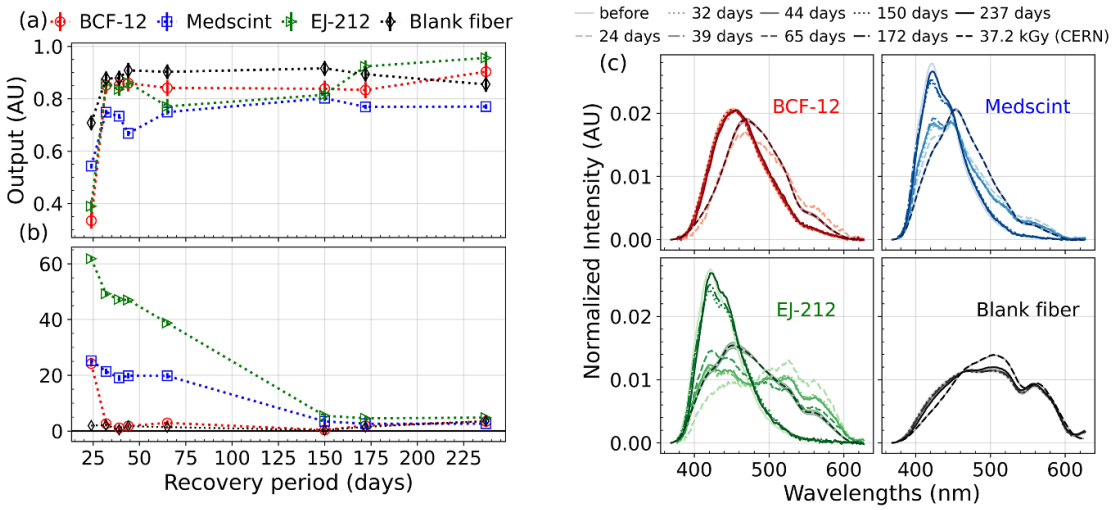

Figure 6. (a) Long-term recovery of light output normalized by initial undamaged response and (b) spectral centroid shift of scintillation spectra, after 37.2 kGy radiation damage. (c) Scintillation spectra measured at different time points after 37.2 kGy radiation damage compared to initial undamaged spectra.

Table 2. Light output and spectral centroid shift of scintillators and blank fiber for the last irradiation at CLEAR and after long-term recovery, compared to initial undamaged light output and spectra respectively.

		BCF-12	Medscint	EJ-212	Blank fiber
Output (%)	Last irradiation (±0.2)	33.4	30.4	37.8	42.7
	Recovery[a] (±2)	85	78	94	89
Centroid shift (nm)	Last irradiation (±1)	18	25	38	7
	Recovery[a] (±1)	2	3	5	2

[a] Recovery values are mean values measured after stabilization of response.

4. Discussion

4.1. Output linearity

In this study, linearity and radiation damage of the response of a 4-channel PSD was investigated, using the UHDR VHEE beam of the CLEAR facility. A saturation of the light output was seen for all scintillators

irradiated with >45 Gy/pulse. During the irradiations, measured spectra were systematically checked to confirm that the Hyperscint RP200 dosimetry platform did not saturate due to the intense light signal. Photodetector saturation can thus be excluded from the possible cause of the output saturation seen at high dose per pulse. IDRs varied non linearly with dose per pulse and depended on pulse length and number of bunches. IDRs ranged from 2.2×10^8 to 4.6×10^9 Gy s^{-1}, the highest dose rates sometimes being used for the lowest dose pulses. This non-linear variation of IDR makes it difficult to isolate the effect of dose per pulse from the effect of IDR. However, as lower IDRs were used for the saturating pulses compared to lower dose pulses, we can exclude IDR dependence as the cause of the loss of linearity at high doses per pulse. The cause of the saturation is unknown but a quenching effect similar to ionization quenching normally seen for high linear energy transfer (LET) radiation could be at play. Ionization quenching is a reduction of the primary excitation efficiency of the scintillator due to high ionization density, leading to a reduction of scintillation efficiency (Beddar and Beaulieu 2016, Christensen and Andersen 2018). At UHDR, high doses delivered in short pulses could produce a similar effect as high LET radiation, thus causing the observed quenching of response.

Output linearity of PSDs has been investigated in previous studies for application in UHDR electron beams. Studies by Ashraf *et al* (2022) and Ciarrochi *et al* (2024) showed no loss of linearity with increasing dose per pulse, but the highest dose measured were respectively 1.1 Gy/pulse and 10 Gy/pulse. Liu *et al* (2024) reported a saturation of the blue and green signals of the Exradin W2 system, housing a BCF-12 scintillator, above dose per pulse of 1.5 Gy, delivered with the 9 MeV beam of a IntraOp Mobetron. The authors hypothesized that the saturation was caused by the electrometer not being designed for high-signal applications, not by effects in the scintillator itself. IDR dependence of the scintillator signal was also observed with the same dose per pulse delivered at different pulse widths, underlining the importance of studying the effects of dose per pulse and dose rate separately. In this study, higher doses of up to 90 Gy/pulse were measured and photodetector saturation was systematically excluded.

Previous work on the application of PSDs to the VHEE UHDR beam at the CLEAR facility by Hart *et al* (2024) reported a loss of linearity above 125.2 and 59.5 Gy/pulse for BCF-12 and Medscint scintillators, respectively. While the same scintillator compositions and similar IDRs were used in our study, a lower saturation limit of (45 ± 1) Gy/pulse was observed and was the same for all scintillators. For the Medscint scintillator, the difference observed falls within the expected dose uncertainties due to positioning and dose calibration. The significant discrepancy observed for BCF-12 cannot be explained at this time.

Interestingly, although significantly less sensitive, the blank fiber outperformed the scintillators in terms of output linearity, as the Cherenkov light signal showed no saturation at the highest dose per pulse of 90 Gy. However, Cherenkov light production is dependent on the volume of fiber irradiated and on the angle relative to the beam, which complicates its direct use for dosimetry (Beaulieu and Beddar 2016). In spite of the loss of linearity at high dose per pulse, the dynamic range of the scintillators tested in this work would be sufficient to cover the range of high dose single fraction used in FLASH radiotherapy. Indeed, doses delivered in most preclinical and early clinical studies are lower than 45 Gy (Vozenin *et al* 2022). For example, a maximum dose of 41 Gy was delivered to cat patients (Vozenin *et al* 2019), a single dose of 15 Gy was used to treat the first human patient (Bourhis *et al* 2019) and doses of 8 Gy were prescribed to human patients in the first FLASH clinical trial, the FAST-01 trial (Mascia *et al* 2023).

4.2. Radiation damage

A total dose of 37.2 kGy was delivered to the 4-channel PSD to assess radiation damage. With accumulation of dose, light output significantly decreased at a mean rate ranging from 1.54 to 1.87%/kGy depending on the probe. After 37.2 kGy, final light output was reduced to 30.4 to 42.7% of initial response, with the blank fiber being the least and the Medscint scintillator the most damaged. Radiation damage also caused a shift of spectra towards longer wavelengths, which could be due to the known yellow discoloration of polymers that appears with accumulation of dose (Zorn 1993). As the probe was shielded from ambient light using black paint, this could not be verified visually during or after irradiations. Importantly, scintillators and blank fiber maintained the same range of linearity to dose per pulse even after significant radiation damage, albeit with a lower slope pointing at lower light output. This allows irradiated PSDs to still be used for dose measurements by recalibrating them before each experiment.

For the scintillators, the rate of light output loss is higher for the first kGys of accumulated dose, with a decrease of more than 20% between 1.4 kGy and 2.1 kGy, while it is much lower and approximately constant after about 10 kGy. Ashraf *et al* (2022) reported a similar effect in their study using the Exradin W1 PSD, with a decrease of 16%/kGy for the first kGy of dose, followed by a lower decrease of about 7%/kGy for subsequent irradiations of about 2 kGy.

Mean decrease of <1.87%/kGy calculated in this study agree well with results from previous work on VHEEs by Hart *et al* (2024), where light output decreases of 1.21 and 1.51%/kGy were measured with

radiation damage of 26.2 and 13.8 kGy for the BCF-12 and Medscint scintillators, respectively. The higher total dose delivered in our study could explain the difference in values. Liu *et al* (2024) observed a light output decrease of about 4%/kGy for a total dose of 8.5 kGy delivered to the Exradin W2 PSD in a single day (∼8 h). The lower decrease we observed could be due to the numerous recovery periods between irradiations that were used in our study.

Scintillators were allowed to rest throughout irradiations to assess short-term recovery of light output and spectral changes. Note that these recovery periods were dictated by the CLEAR beam availability. At 1 h rest time and 7.1 kGy total accumulated dose, the light output was recovered at a rate of about 4.6%/h for BCF-12, 2.7%/h for Medscint, 1.9%/h for EJ-212 and 0.64%/h for blank fiber. At 26 h and 28.2 kGy, recovery rate was about 0.076, 0.23, 0.25 and 0.26%/h for BCF-12, Medscint, EJ-212 and blank fiber respectively. This suggests that recovery depends on rest duration but also on accumulated dose. The lack of correlation between light output and spectral recovery also indicates that different processes may be implicated in recovery of output and spectral changes. While polystyrene and PVT based scintillators follow a similar behavior with radiation damage, the PMMA blank fiber differs, as shown in figure 5 a). Type of base matrix (i.e. polystyrene, PVT or PMMA) therefore also has an effect on the radiation damage and recovery processes.

The processes of radiation damage in polymers were extensively studied in the 1990s (see Bross and Pla-Dalmau 1992, Zorn 1993, Biagtan *et al* 2001) and more recently (see Kharzheev 2019, Kronheim *et al* 2024, Papageorgakis *et al* 2024). According to these studies, radiation can break chemical bonds in polymers, which creates free radicals. These radicals act as color centers and absorb scintillation photons, consequently degrading intrinsic scintillation light output as well as transmission in the scintillator particularly for long samples. This causes a loss in light output as well as a yellow discoloration that gets darker with increasing absorbed dose. It is important to note that these studies primarily focused on radiation damage caused by large accumulation of dose (∼100 kGy) delivered continuously over long periods, with dose rates significantly lower than those in the FLASH UHDR regime. While radiation damage processes in UHDR conditions could be different, the output and spectral changes that were observed in this work agree with what these studies predicted.

Scintillators with wavelength shifters that emit at longer wavelengths are more radiation hard, due to the absorption centers created after irradiation that absorb light mostly in the UV and blue regions (Zorn 1993, Kharzheev 2019). This was observed experimentally with the green channel reading of the Exradin W2 PSD being more radiation hard than the blue channel in the study by Liu *et al* (2024). Future work will further explore the use of these types of scintillators in UHDR beams.

4.3. Long-term recovery

Residual permanent damage of light output of 6%–22% remained after recovery, with the Medscint scintillator being the most damaged. These values are comparable to the 5%–15% range of residual (irrecoverable) light yield loss reported in the review by Kharzheev (2019) for plastic scintillators irradiated with doses under 1 MGy. Spectral changes were completely recovered for scintillators, at a slower rate for the polystyrene based Medscint and PVT based EJ-212. However, no data points were collected between 65 and 150 days of recovery, so complete output and spectral recovery may have occurred sooner for these scintillators. The output stabilization time for the Medscint channel is particularly ambiguous to determine due to this important time gap but is between 65 and 150 days.

Radiation damage of scintillators is mostly due to damage to the polymer matrix and not to the fluor itself (Bross and Pla-Dalmau 1992, Zorn 1993, Kharzheev 2019). This causes a degradation of the scintillation light output and of the light transmission properties. Oxygen-driven annealing occurs after irradiation and allows recovery of temporary damage. The higher diffusion rate of oxygen in polystyrene compared to PVT could explain the faster recovery observed for polystyrene based BCF-12 (Kharzheev 2019). Although the Medscint scintillator is also polystyrene based, its composition includes a dopant optimized to reduce energy dependence and compensate for quenching effects (Gingras *et al* 2025). This dopant may influence the recovery process, potentially explaining the slower recovery compared to the BCF-12, which shares the same polystyrene matrix but lacks the dopant.

The complete spectral recovery observed across all channels suggests that radiation damage caused only a transient yellowing of the scintillators or the PMMA optical fibers connected to them. The observed spectral changes could have originated from either damage to the scintillator itself or to the optical fiber coupled with the plastic scintillators. Discriminating between these two sources would have required light transmission measurements in parallel with the light output measurements. Unfortunately, these measurements demanded the destruction of the 4-channel PSD, which was impossible before stabilization of the output and spectral response. After stabilization, measurement of the transmission of light through the optical fibers were conducted but showed no significant difference from transmission of non-irradiated segments of the same fibers. This was to be expected based on the results presented in figure 6 and table 2, where a complete

spectral recovery was already noted for the blank fiber channel. For future work, a probe design where transmission measurements can be conducted in parallel with light output and spectral measurements will be considered to allow discrimination between damage to the optical fiber and damage to the scintillator itself.

4.4. Limitations

The presented results are compounded by dose uncertainties due to beam delivery. The CLEAR beamline is strictly experimental and has a high degree of uncertainty in dose delivery compared to a clinical linear accelerator. Indeed, beam parameters, including the beam size (see figure 3(c)), the dose delivered per charge and the beam positioning, varied each day and even throughout a given day. To mitigate the effect of these variations, conducting a film measurement before each scintillator measurement would have been necessary. Instead, due to logistical reasons, a few film measurements per day were performed to provide an estimate of the beam parameters for that day. Visual probe positioning in the Gaussian beam also represented a source of uncertainty and a simulation was used to estimate it. To limit uncertainties, PSD response should be first characterized on a beam with more controlled parameters. Notably, a flat beam of constant size would significantly reduce positioning uncertainty. Moreover, even after correction for the Gaussian beam using the off-axis factors, stem light removal by subtraction of the blank fiber channel still induced uncertainty. Future work could explore a more accurate method for stem light subtraction, for instance the hyperspectral method described by others (Archambault *et al* 2012, Therriault-Proulx *et al* 2013), but this would require a kV source, which is not available at CLEAR presently.

This study is limited by the discrepancy in the measured BCF-12 saturation limit from that reported by Hart *et al* (2024), although the two studies are in agreement for the Medscint scintillators. Different photodetector systems were used in both studies, but photodetector saturation was ruled out, as spectra were systematically checked for saturation effects. Hart *et al* used smaller beam sizes with steeper dose gradients, making precise alignment more challenging. However, positioning uncertainties alone cannot explain the large difference observed for BCF-12 (45 Gy vs. 125 Gy). A beam drift of about 7 mm would be needed to explain the nearly threefold dose difference, which is not probable due to regular positioning verification and reproducibility of the holder position. Pulse lengths and dose rates per pulse were similar between studies, but other beam parameters might have differed. In our study, charge to dose calibration factors ranged from 0.6 to 1.13 Gy/nC, while in Hart *et al* they were around 2 Gy/nC, meaning their beam delivered a higher dose for the same charge. The effect of these variations on PSD response is unclear and the incomplete recording of beam parameters complicates the identification of a clear trend. We therefore cannot currently provide an explanation for the discrepancy between the two studies, and additional measurements with a BCF-12 scintillator are needed to investigate this aspect.

5. Conclusion

In this study, we investigated the output linearity and radiation damage of PDSs irradiated up to 37.2 kGy by a 200 MeV electron beam with dose rate in pulse up to 4×10^9 Gy s^{-1} at the CERN CLEAR facility. To our knowledge, this experiment represents the first systematic study of radiation damage and recovery of PSDs under UHDR conditions. Polystyrene and PVT based scintillators were linear to dose per pulse until approximately 45 Gy/pulse, while PMMA blank fiber response was linear up to the maximal dose measured of 90 Gy/pulse. Scintillator response saturation was observed above (45 ± 1) Gy/pulse and could be attributed to a quenching of the scintillation efficiency at high doses per pulse. Radiation damage caused a mean decrease of light output under 1.87%/kGy for scintillators and blank fiber, as well as a spectral shift towards longer wavelengths. Linearity below 45 Gy/pulse was maintained even after a significant delivered dose of 37.2 kGy, which allows the reuse of damaged PSD following a recalibration. Short-term ($<$100 h) recovery of light output was reported and depended on rest duration and accumulated dose at the time of recovery. Long-term ($<$172 days) recovery of output and spectral changes was significant. After stabilization of response, residual permanent damage of light response of 6-22% remained, while spectral recovery was complete.

Future work will investigate radiation damage and recovery of green-emitting scintillators that have been shown to be more radiation hard. To discriminate damage to the scintillator from damage to the coupled PMMA optical fiber, a novel probe design will be explored, allowing optical fiber light transmission measurements to be conducted in parallel with scintillator output and spectra measurements.

Data availability statement

The data cannot be made publicly available upon publication because they are not available in a format that is sufficiently accessible or reusable by other researchers. The data that support the findings of this study are available upon reasonable request from the authors.

Acknowledgments

The authors would like to thank the Medscint team for their assistance in designing and constructing the PSD used in the experiments and for their contributions to the analysis of the results. We also extend our gratitude to the CLEAR team for operating the beam during the experiments and for their continued support afterward.

This research was funded in part by the Natural Sciences and Engineering Council (NSERC) Discovery Grants (RGPIN-2019-05038) held by Dr Luc Beaulieu, as well as the NSERC Discovery Grants (RGPIN-2021-03516 and RGPAS-2021-00019) and the Canada Research Chairs program (CRC-2019-00039) held by Dr Magdalena Bazalova-Carter. First-author Cloé Giguère was also supported by a CGS M scholarship from NSERC and a Mitacs Accelerate Fellowship.

ORCID iDs

Cloé Giguère https://orcid.org/0009-0003-9520-8305
Alexander Hart https://orcid.org/0000-0002-0547-5887
Joseph Bateman https://orcid.org/0000-0002-5967-6748
Pierre Korysko https://orcid.org/0000-0002-7878-2298
Magdalena Bazalova-Carter https://orcid.org/0000-0002-9365-2889
Luc Beaulieu https://orcid.org/0000-0003-0429-6366

References

Andreo P, Burns D T, Nahum A E, Seuntjens J and Attix F H 2017 *Fundamentals of Ionizing Radiation Dosimetry* 2nd edn (Wiley-VCH)

Archambault L, Therriault-Proulx F, Beddar S and Beaulieu L 2012 A mathematical formalism for hyperspectral, multipoint plastic scintillation detectors *Phys. Med. Biol.* **57** 7133

Archer J, Enbang Li, Davis J, Cameron M, Rosenfeld A and Lerch M 2019 High spatial resolution scintillator dosimetry of synchrotron microbeams *Sci. Rep.* **9** 6873

Ashraf M, Rahman M, Zhang R, Williams B, Gladstone D, Pogue B and Bruza P 2020 Dosimetry for FLASH radiotherapy: a review of tools and the role of radioluminescence and Cherenkov emission *Front. Phys.* **8** 328

Ashraf M R, Rahman M, Cao X, Duval K, Williams B B, Jack Hoopes P, Gladstone D J, Pogue B W, Zhang R and Bruza P 2022 Individual pulse monitoring and dose control system for pre-clinical implementation of FLASH-RT *Phys. Med. Biol.* **67** 095003

Bateman J J *et al* 2024 Development of a novel fibre optic beam profile and dose monitor for very high energy electron radiotherapy at ultrahigh dose rates *Phys. Med. Biol.* **69** 085006

Bazalova-Carter M, Bradley Q, Palma B, Hårdemark B, Hynning E, Jensen C, Maxim P G and Loo B W 2015 Treatment planning for radiotherapy with very high-energy electron beams and comparison of VHEE and VMAT plans *Med. Phys.* **42** 2615–25

Beaulieu L and Beddar S 2016 Review of plastic and liquid scintillation dosimetry for photon, electron and proton therapy *Phys. Med. Biol.* **61** R305–43

Beaulieu L, Goulet M, Archambault L and Beddar S 2013 Current status of scintillation dosimetry for megavoltage beams *J. Phys.: Conf. Ser.* **444** 012013

Beddar S and Beaulieu L 2016 Scintillation Dosimetry (Imaging in Medical Diagnosis and Therapy) (CRC Press, Taylor & Francis Group)

Biagtan E, Goldberg E, Stephens R, Valeroso E, Calves M and Harmon J 2001 Polymer Scintillators: Continuous versus Intermittent Gamma Irradiation Effects *Optical Polymers: Fibers and Waveguides* (*ACS Symposium Series* vol 795) 795 (American Chemical Society)

Bourgouin A, Schüller A, Hackel T, Kranzer R, Poppinga D, Kapsch R-P and McEwen M 2020 Calorimeter for real-time dosimetry of pulsed ultra-high dose rate electron beams *Front. Phys.* **8** 567340

Bourhis J, Ozsahin M, Bochud F, Germond J-F, Moeckli R and Vozenin M-C 2019 Treatment of a first patient with FLASH-radiotherapy *Radiother. Oncol.* **139** 18–22

Bross A D and Pla-Dalmau A 1992 Radiation damage of plastic scintillators *IEEE Trans. Nucl. Sci.* **39** 1199–204

Cecchi D D, Therriault-Proulx F, Lambert-Girard S, Hart A, Macdonald A, Pfleger M, Lenckowski M and Bazalova-Carter M 2021 Characterization of an x-ray tube-based ultrahigh dose-rate system for in vitro irradiations *Med. Phys.* **48** 7399–409

Christensen J B and Andersen C E 2018 Relating ionization quenching in organic plastic scintillators to basic material properties by modelling excitation density transport and amorphous track structure during proton irradiation *Phys. Med. Biol.* **63** 195010

Ciarrocchi E *et al* 2024 Plastic scintillator-based dosimeters for ultra-high dose rate (UHDR) electron radiotherapy *Phys. Medica* **121** 103360

Clements N, Esplen N and Bazalova-Carter M 2023 A feasibility study of ultra-high dose rate mini-GRID therapy using very-high-energy electron beams for a simulated pediatric brain case *Phys. Med.* **112** 102637

DesRosiers C, Moskvin V, Bielajew A F and Papiez L 2000 150-250 meV electron beams in radiation therapy *Phys. Med. Biol.* **45** 1781–805
Diffenderfer E S, Sørensen B S, Mazal A and Carlson D J 2022 The current status of preclinical proton FLASH radiation and future directions *Med. Phys.* **49** 2039–54
Duchaine J, Markel D and Bouchard H 2022 A probabilistic approach for determining Monte Carlo beam source parameters: I. Modeling of a CyberKnife M6 unit *Phys. Med. Biol.* **67** 045007
Esplen N, Egoriti L, Paley B, Planche T, Hoehr C, Gottberg A and Bazalova-Carter M 2022 Design optimization of an electron-to-photon conversion target for ultra-high dose rate x-ray (FLASH) experiments at TRIUMF *Phys. Med. Biol.* **67** 105003
Esplen N, Mendonca M S and Bazalova-Carter M 2020 Physics and biology of ultrahigh dose-rate (FLASH) radiotherapy: A topical review *Phys. Med. Biol.* **65** 23TR03
Favaudon V *et al* 2014 Ultrahigh dose-rate FLASH irradiation increases the differential response between normal and tumor tissue in mice *Sci. Trans. Med.* **6** 245ra93
Fischer J, Whitmore L, Desrosiers C, Sheehy S and Bazalova-Carter M 2024 Very high-energy electrons as radiotherapy opportunity *Eur. Phys. J. Plus* **139** 728
Giguère C, Hart A, Bateman J, Korysko P, Farabolini W, LeChasseur Y, Bazalova-Carter M and Beaulieu L 2024 Real-time plastic scintillation dosimetry of ultra-high dose rate very high energy electrons (VHEE) at CERN CLEAR facility *J. Phys.: Conf. Ser.* **2799** 012016
Gingras L 2025 Field output correction factors using a fully characterized plastic scintillation detector Med. Phys. 1-18
Grazia Ronga M, Cavallone M, Patriarca A, Maia Leite A, Loap P, Favaudon V, Créhange G and De Marzi L 2021 Back to the future: very high-energy electrons (VHEEs) and their potential application in radiation therapy *Cancers* **13** 4942
Hart A *et al* 2024 Plastic scintillator dosimetry of ultrahigh dose-rate 200 MeV electrons at CLEAR *IEEE Sens. J.* **24** 14229–37
Hart A, Cecchi D, Giguere C, Larose F, Therriault-Proulx F, Esplen N, Beaulieu L and Bazalova-Carter M 2022 Lead-doped scintillator dosimeters for detection of ultrahigh dose-rate x-rays *Phys. Med. Biol.* **67** 105007
Jaccard M, Petersson K, Buchillier T, Germond J-F, Teresa Durán M, Vozenin M-C, Bourhis J, Bochud F O and Bailat C 2017 High dose-per-pulse electron beam dosimetry: Usability and dose-rate independence of EBT3 Gafchromic films *Med. Phys.* **44** 725–35
Jolly S, Owen H, Schippers M and Welsch C 2020 Technical challenges for FLASH proton therapy *Phys. Med.* **78** 71–82
Jorge P G *et al* 2019 Dosimetric and preparation procedures for irradiating biological models with pulsed electron beam at ultra-high dose-rate *Radiother. Oncol.* **139** 34–39
Karsch L, Beyreuther E, Burris-Mog T, Kraft S, Richter C, Zeil K and Pawelke J 2012 Dose rate dependence for different dosimeters and detectors: TLD, OSL, EBT films and diamond detectors *Med. Phys.* **39** 2447–55
Kharzheev Y N 2019 Radiation hardness of scintillation detectors based on organic plastic scintillators and optical fibers *Phys. Part. Nucl.* **50** 42–76
Korysko P n.d. C-Robot (available at: http://pkorysko.web.cern.ch/C-Robot/C-Robot.html)
Kronheim B, Belloni A, Edberg T K, Eno S C, Howe C Palmer C Papageorgakis C, Paranjpe M and Sriram S 2024 Reduction of light output of plastic scintillator tiles during irradiation at cold temperatures and in low-oxygen environments *Nucl. Instrum. Methods Phys. Res.* A **1059** 168922
Liu K, Holmes S, Hooten B, Schüler E and Beddar S 2024 Evaluation of ion chamber response for applications in electron FLASH radiotherapy *Med. Phys.* **51** 494–508
Liu K, Holmes S, Schüler E and Beddar S 2024 A comprehensive investigation of the performance of a commercial scintillator system for applications in electron FLASH radiotherapy *Med. Phys.* **51** 4504–12
Mascia A E *et al* 2023 Proton FLASH radiotherapy for the treatment of symptomatic bone metastases: the FAST-01 nonrandomized trial *JAMA Oncol.* **9** 62–69
McManus M, Romano F, Lee N D, Farabolini W, Gilardi A, Royle G, Palmans H and Subiel A 2020 The challenge of ionisation chamber dosimetry in ultra-short pulsed high dose-rate Very High Energy Electron beams *Sci. Rep.* **10** 9089
Montay-Gruel P *et al* 2017 Irradiation in a flash: Unique sparing of memory in mice after whole brain irradiation with dose rates above 100 Gy s^{-1} *Radiother. Oncol.* **124** 365–9
Montay-Gruel P *et al* 2019 Long-term neurocognitive benefits of FLASH radiotherapy driven by reduced reactive oxygen species *Proc. Natl Acad. Sci.* **116** 10943–51
Papageorgakis C, Aamir M Y, Belloni A, Edberg T K, Eno S C, Kronheim B and Palmer C 2024 Effects of oxygen on the optical properties of phenyl-based scintillators during irradiation and recovery *Nucl. Instrum. Methods Phys. Res.* A **1059** 168977
Petersson K, Jaccard M, Germond J-F, Buchillier T, Bochud F, Bourhis J, Vozenin M-C and Bailat C 2017 High dose-per-pulse electron beam dosimetry — a model to correct for the ion recombination in the Advanced Markus ionization chamber *Med. Phys.* **44** 1157–67
Poirier Y, Junliang X, Mossahebi S, Therriault-Proulx F and Sawant A 2022 Technical note: Characterization and practical applications of a novel plastic scintillator for online dosimetry for an ultrahigh dose rate (FLASH) *Med. Phys.* **49** 4682–92
Poppinga D, Kranzer R, Farabolini W, Gilardi A, Corsini R, Wyrwoll V, Khee Looe H, Delfs B, Gabrisch L and Poppe B 2020 VHEE beam dosimetry at CERN Linear Electron Accelerator for Research under ultra-high dose rate conditions *Biomed. Phys. Eng. Express* **7** 015012
Romano F, Bailat C, Gonçalves Jorge P, Lloyd Franz Lerch M and Darafsheh A 2022 Ultra-high dose rate dosimetry: challenges and opportunities for FLASH radiation therapy *Med. Phys.* **49** 4912–32
Santos T, Ventura T, Capela M, Mateus J and do Carmo Lopes M 2021 A protocol for absolute dose verification of SBRT/SRS treatment plans using Gafchromic™ EBT-XD films *Phys. Med.* **82** 150–7
Sarti A *et al* 2021 Deep seated tumour treatments with electrons of high energy delivered at FLASH rates: the example of prostate cancer *Front. Oncol.* **11** 777852
Schulte R *et al* 2023 Transformative Technology for FLASH Radiation Therapy *Appl. Sci.* **13** 5021
Sjobak K *et al* 2019 Status of the CLEAR electron beam user facility at CERN *10th Int. Partile Accelerator Conf.* (*Melbourne, Australia, 2019*) pp 983–6
Therriault-Proulx F, Beaulieu L, Archambault L and Beddar S 2013 On the nature of the light produced within PMMA optical light guides in scintillation fiber-optic dosimetry *Phys. Med. Biol.* **58** 2073–84
Tobias Böhlen T, Germond J-F, Traneus E, Bourhis J, Vozenin M-C, Bailat C, Bochud F and Moeckli R 2021 Characteristics of very high-energy electron beams for the irradiation of deep-seated targets *Med. Phys.* **48** 3958–67

Vozenin M-C et al 2019 The Advantage of FLASH Radiotherapy Confirmed in Mini-pig and Cat-cancer Patients *Clin. Cancer Res.* **25** 35–42
Vozenin M-C, Bourhis J and Durante M 2022 Towards clinical translation of FLASH radiotherapy *Nat. Rev. Clin. Oncol.* **19** 791–803
Whitmore L, Mackay R I, van Herk M, Jones J K and Jones R M 2021 Focused VHEE (very high energy electron) beams and dose delivery for radiotherapy applications *Sci. Rep.* **11** 14013
Yang Y et al 2024 FLASH radiotherapy using high-energy x-rays: current status of PARTER platform in FLASH research *Radiother. Oncol.* **190** 109967
Zhang G, Zhang Z, Gao W and Quan H 2023 Treatment planning consideration for very high-energy electron FLASH radiotherapy *Phys. Med.* **107** 102539
Zorn C 1993 A pedestrian's guide to radiation damage in plastic scintillators *Nucl. Phys.* B **32** 377–83